



HAL
open science

An investigation into electrical ageing of insulating polymers by detection of charge injection under alternative divergent field

A. Hadid, C. Laurent, M. Mammeri, R. Clavreul, F. Duchateau, J. Berdala

► **To cite this version:**

A. Hadid, C. Laurent, M. Mammeri, R. Clavreul, F. Duchateau, et al.. An investigation into electrical ageing of insulating polymers by detection of charge injection under alternative divergent field. *Journal de Physique III*, 1994, 4 (1), pp.35-53. 10.1051/jp3:1994111 . jpa-00249091

HAL Id: jpa-00249091

<https://hal.science/jpa-00249091>

Submitted on 4 Feb 2008

HAL is a multi-disciplinary open access archive for the deposit and dissemination of scientific research documents, whether they are published or not. The documents may come from teaching and research institutions in France or abroad, or from public or private research centers.

L'archive ouverte pluridisciplinaire **HAL**, est destinée au dépôt et à la diffusion de documents scientifiques de niveau recherche, publiés ou non, émanant des établissements d'enseignement et de recherche français ou étrangers, des laboratoires publics ou privés.

Classification

Physics Abstracts

77.50 — 72.20H — 81.40G — 81.70

An investigation into electrical ageing of insulating polymers by detection of charge injection under alternative divergent field

A. Hadid ⁽¹⁾, C. Laurent ⁽¹⁾, M. Mammeri ⁽¹⁾, R. Clavreul ⁽²⁾, F. Duchateau ⁽²⁾ and J. Berdala ⁽³⁾

⁽¹⁾ Laboratoire de Génie Electrique, CNRS URA 304, Université Paul Sabatier, Toulouse, France

⁽²⁾ Electricité de France, Direction des Etudes et Recherches, Les Renardières, Moret-sur-Loing, France

⁽³⁾ Câbles-Pirelli, Direction des Recherches et Développement, Paron, France

(Received 21 June 1993, revised 28 September 1993, accepted 7 October 1993)

Résumé. — Le but de l'étude est la compréhension du vieillissement électrique des isolants polymères sous tension alternative et en l'absence de toute décharge partielle, i.e. lorsqu'il n'existe aucune cavité gazeuse interne à l'isolant. Nous avons utilisé des électrodes de type aiguille afin d'augmenter localement les gradients de tension moyens et de simuler les défauts amplificateurs de champ. Une technique de mesure de la quantité de charge injectée sous tension alternative dans l'isolant a été mise au point. Elle permet l'étude de la transition entre le régime électroluminescent exempt de décharges électriques et la phase dans laquelle sont détectées des décharges partielles de très faible amplitude (premiers instants de la propagation de l'arborescence électrique). Le seuil de détection des phénomènes électriques est de 0,01 pC. La transition à l'arborescence est aussi étudiée par une méthode optique. L'isolant est un polyéthylène basse densité utilisé dans le domaine des câbles de transport d'énergie tandis que les électrodes sont soit métalliques, soit semi-conductrices. L'étude statistique des temps de transition à l'arborescence montre que l'extrémité de l'électrode ne peut pas être considérée comme une surface injectante homogène. Il en découle que la valeur des champs électriques calculée à partir du rayon de courbure mesuré des électrodes n'est qu'une valeur macroscopique. Les essais par la méthode de l'aiguille doivent être analysés par la statistique de Weibull en prenant en compte l'existence du paramètre de localisation.

Abstract. — Our aim is to understand the electrical ageing of insulating polymeric materials under a.c. voltage and in discharge-free situation, i.e. in the absence of any pre-existing gaseous cavities in the bulk of the dielectric. In this report, we use a needle electrode moulded into the insulant to simulate defects producing local field enhancement. An experimental technique for measuring the charge flow injected by the needle into the dielectric under a.c. voltage is described. The transition between the discharge-free electroluminescent state to micro-partial discharge state (early electrical tree propagation phase) is investigated with a sensitivity reaching 0.01 pC. Optical diagnosis is carried out simultaneously. Special emphasis is given to synthetic insulation of power cables. Low-density polyethylene is used as a dielectric with moulded metallic needle electrode. Semi-conducting electrodes prepared from the shield of a cable are also used in this investigation. Statistics on times to tree inception show that the needle tip cannot be considered as a homogeneous injecting surface. The conclusion is double : (i) the onset field for massive charge transfer derived from the measured curvature radius of the needle is not the absolute value and (ii) the discussion of the results obtained by a needle test must include a Weibull statistical analysis with determination of the location parameter.

1. Introduction.

Ageing can be defined as a slow and non-reversible evolution of material's properties due to the inherent instability of the material itself or to the effect of environmental parameters. In this report, we are dealing with stable polymeric materials as those used for the insulating of power cables. Degradation due to electrical discharges at the surface of the insulant does not fall within the scope of the paper. Also excluded are water treeing related phenomena, which concern water impregnated polymers. Under normal operating conditions, polyethylene insulations of power cables are submitted to average voltage gradient in the range of 10 kV/mm, depending on the type of polyethylene. In this context, two situations can lead to dielectric ageing : the presence of gaseous cavities, in which partial discharges can take place, or the existence of field-enhancing defects leading to some high field effects. In both situations, ageing ends up with the generation of electrical treeing leading to rapid breakdown [1]. Our aim is to understand ageing in discharge-free situation under 50 Hz-a.c. diverging field.

Space charges play a very important part when present around field-distorting defects. Apart from the reduction or enhancement of the local field by the presence of homo- or hetero-charges, charge generation is expected to be directly involved in the ageing process [2-4]. Indirect evidence of space charge injection from a needle electrode into a dielectric was provided by measuring the light appearing by electroluminescence in polyethylene under a.c. stress prior to partial discharge detection and tree propagation [5]. The origin of the light has been thoroughly discussed in different papers : it may be due either to hot electron processes, or to some recombination process that does not involve hot carriers. In both cases, chemical deterioration of the dielectric follows, since energy in the low electron-volt range (optical region) is dumped into the material. Ageing in a divergent field appears to be caused by the direct (hot electron impact) or indirect (recombination) effect of space charge injection which causes cumulative deterioration and fatigue failure of the polymer. It is therefore very important to be able to measure the charge flow in order to anticipate the ability of a given material to bear high electrical stresses without degradation. This question is of major interest in the domain of synthetic insulations of power cables since there is a tendency to increase the service voltage gradients. Indeed, it is imperative to keep a high degree of reliability.

The concept of a critical field level above which fast charge carrier transport occurs was developed by Zeller and Schneider in the Field-Limiting Space Charge model [2]. The determination of this quantity is of great technical importance, since below this threshold, ageing is not expected to take place [6]. In one of our previous works [7], the idea was put forward that charge flow can be detected in a double-needle electrode configuration if the complex components of the currents are accurately compensated. Owing to the non-linearity of the charge transfer process *versus* voltage, strong injection onset can be detected. In our previous set-up [7], we used two identical samples submitted to two different voltage levels to compensate the losses unrelated to charge injection. In order to improve this method, we have built a new detector with only one sample and with a better overall sensitivity, so that the determination of the critical field is better too. In contrast with the set-up described in reference [7], the measurements and the data processing are fully automated by means of a personal computer. Moreover, the set-up allows to detect micro-partial discharges in the transition phase between electrical tree initiation and propagation, with a sensitivity reaching 0.01 pC.

In a first part of the paper, we briefly remind the theoretical model of the Field-Limiting Space Charge and give the principle of measurement. The charge detector is described in a second part. The experimental results obtained on low-density polyethylene samples with metallic or semi-conducting needle electrodes are discussed in a third part.

2. Theoretical model and principle of measurement.

2.1 FIELD-LIMITING SPACE CHARGE (FLSC) MODEL. — Zeller and Schneider [2] have proposed the concept of a field-limiting space charge which takes into account the screening effect of a space charge cloud on the electric field at the injecting point. They propose that above a critical field, E_c , the mobility of carriers in polymers be increased sharp from typical low values (« hopping » mobility ranging about 10^{-6} cm²/V.s) to those encountered in band transport (mobility edge value of about 1 cm²/V.s). This change in mobility is so great that a reasonable approximation can be :

$$\begin{aligned} \mu &= 0 & E < E_c \\ \mu &= \mu_\infty & E > E_c \end{aligned}$$

where μ_∞ is the high-field limiting value of mobility μ .

The FLSC model applies to the situation in which an electrode is able to inject charge when the applied voltage exceed a limiting value E_{inj} . In the absence of a mobility transition, space charge is injected above E_{inj} and diffuses throughout insulation until, in equilibrium, the field at the injecting point is reduced to E_{inj} . This behaviour corresponds to the so-called space charge limited conduction equilibrium [8]. The introduction of a mobility transition changes drastically the above : in the most realistic situation where $E_c > E_{inj}$, initially injected space charge moved rapidly away from the electrode under the influence of the local field exceeding E_c , while simultaneously reducing the field in the region behind the space charge boundary. The charges then get localized in that part of the dielectric where the field is below E_c . The charge flow will stop if $E = E_c$ in the space-charge region and $E < E_c$ outside. In a FLSC model, the space-charge formation is mobility and not injection limited, i.e. the space charge boundary can move forward across the insulation due to its high mobility prior to space charge control of the current. This implies the size of the space charge cloud will increase with the voltage applied to the injecting point.

The concept of a FLSC is simple and makes computations of space charge possible without knowing any parameter such as mobilities and trap concentrations. This is the main interest of this model which can be used to estimate the amount of injected charge, but is otherwise too simplistic to take into account all the interface parameters capable of influencing charge transfer at a metal-dielectric contact. This model allows to forecast that the experimental charge Q_{exp} should increase quadratically with voltage according to the following expression [6] :

$$Q_{exp} = g \epsilon_r \epsilon_0 E_c r^2 (V/V_c - 1)^2$$

where g is a correcting factor taking into account the geometry of the injecting site, ϵ_r and ϵ_0 stand for the dielectric constant of the insulant and vacuum, r is the curvature radius of the injecting point, V the voltage applied and V_c the voltage needed to reach E_c at the injecting point.

2.2 PRINCIPLE OF MEASUREMENT. — When a dielectric is submitted to a voltage V for which copious charge injection occurs, an extra contribution of the charge flow to the electrode sets in. In a FLSC model, the injected charge contribution Q_{inj} becomes a measurable quantity above E_c but is difficult to extract since the capacitive charge is greater by several orders of magnitude. In order to decrease it significantly, a double-needle electrode configuration was chosen, as shown in figure 1. In the case of polyethylene and for the same electrode spacing $d = 1$ mm, the capacity of a point-to-plane configuration is 10 pF, whereas the capacity of a double-needle system is 0.1 pF. The maximum electrostatic field (no space charge effect) at

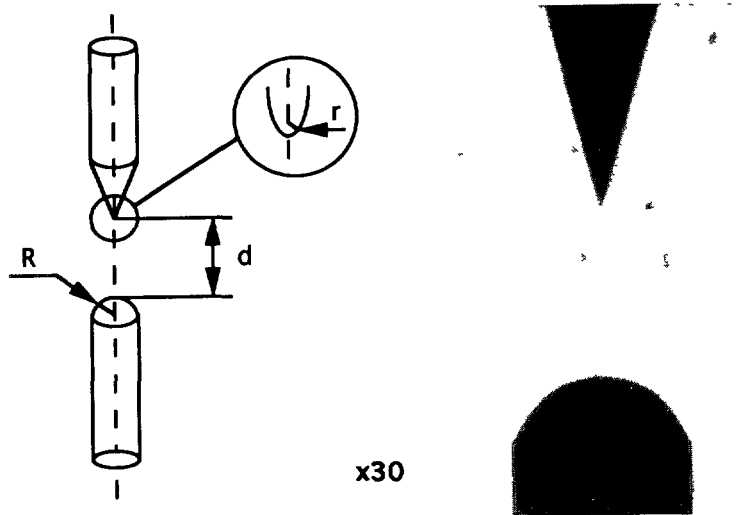


Fig. 1. — Asymmetric double needle electrode configuration : specimen parameters and microscopic observation of metallic needles moulded into polyethylene. r : between 2.5 and 4 μm ; R : 500 μm ; d : 1 mm. Capacitance of additive-free, low density polyethylene sample : 0.1 pF.

the needle tip is given by [9] :

$$E_{\max} = 2V / [r \ln (2d(1 + 2d/R)/r)]$$

where R stands for the curvature radius of the blunt needle electrode.

The measurement of Q_{inj} is based on the separate compensation of the capacitive and dissipative components of the current flowing in the circuit at low input voltage, the injected charge being neglected at this field strength (for $V = 100 V_{\text{peak}}$, $E = 80 \text{ kV}_{\text{peak}}/\text{cm}$ for a 3 μm needle tip radius and a 1 mm gap). Assuming a linear dependence of these components *versus* voltage, the injected charge flow appears as a non-linear contribution to the total charge.

3. Experimental.

3.1 THE CHARGE DETECTOR. — The schema of the charge detector is given in figure 2. The capacitive charge of the sample $Q_c = CV$ is compensated by adding another charge $Q'_c = -Q_c$. This charge is generated at the terminals of capacitor C' , to which a low voltage $-G \cdot V/1000$ is applied, G being the operational amplifier gain. The residual dissipative current I_{dis} representing the losses of the polymer is amplified by using a very sensitive operational amplifier (sensitivity : 100 mV/pC, polarization current : 40 fA) working as a charge-voltage converter with a feedback capacitor $C_f = 10$ pF. The output voltage V_1 is given by :

$$V_1 = - (1/C_f) \int I_{\text{dis}}(t) dt = - Q_{\text{dis}}/C_f.$$

The dissipative component Q_{dis} is subsequently compensated by adding an electronically generated voltage $V_2 = + Q_{\text{dis}}/C_f$ to the voltage V_1 . For most of our measurements on low density polyethylene, the polymer losses were so low that it was not necessary to balance them. In this case, the signal is taken at the output of the charge amplifier.

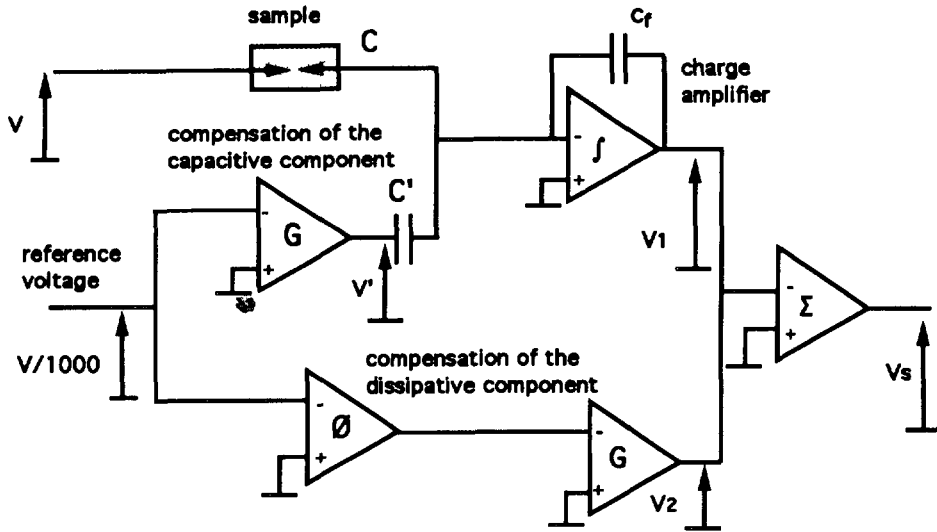


Fig. 2. — Schematic of the charge detector.

The electronic components of the detector are selected for their good electrical characteristics, high thermal stability and very low intrinsic noise. The detector is protected from electromagnetic interference and other kinds of electrical power line instabilities. After tuning the circuit, and accounting for the background electrical noise in the set-up, the output voltage V_s of the detector is :

$$V_s = 500 \mu V_p \quad \text{for } V < V_c$$

$$V_s = Q_{inj}/C_f \quad \text{for } V > V_c.$$

Considering the 10 pF feedback capacitance, the noise level is equivalent to a charge of ≈ 0.005 pC.

3.2 THE WHOLE SET-UP WITH OPTICAL DETECTION. — The whole set-up is given in figure 3. The high voltage supply is an amplifier with a gain of 1 000, excited by a function generator. The reference signal $V/1\ 000$ used in the compensation stages is linear and in phase with the high voltage waveform. The charge detector output voltage is recorded on one of the two synchronous tracks on a 20 kHz sampling frequency data acquisition card. The second track is used to record the excitation waveform.

The voltage at the sample ends is increased by steps. At each voltage level, the system records the output signal and the reference signal (the excitation voltage). All the measurement parameters are computerized : excitation frequency, initial and final voltages, voltage step amplitude and duration.

The bridge is tuned at a given frequency by accurately adjusting the amplifier gain of each compensation stage. Then, an automatic program is run, generating basically two different types of information : (i) the charge waveform *versus* time at each voltage step, and (ii) the curve $Q_{inj} = f(V)$ of the peak charge amplitude *versus* voltage. For the latter, the charge is recorded during a given number of cycles at each voltage step.

An optical detection is provided by mounting a photomultiplier tube focussed on the needle tip. This system allows to discriminate between discharge-free regime and the early

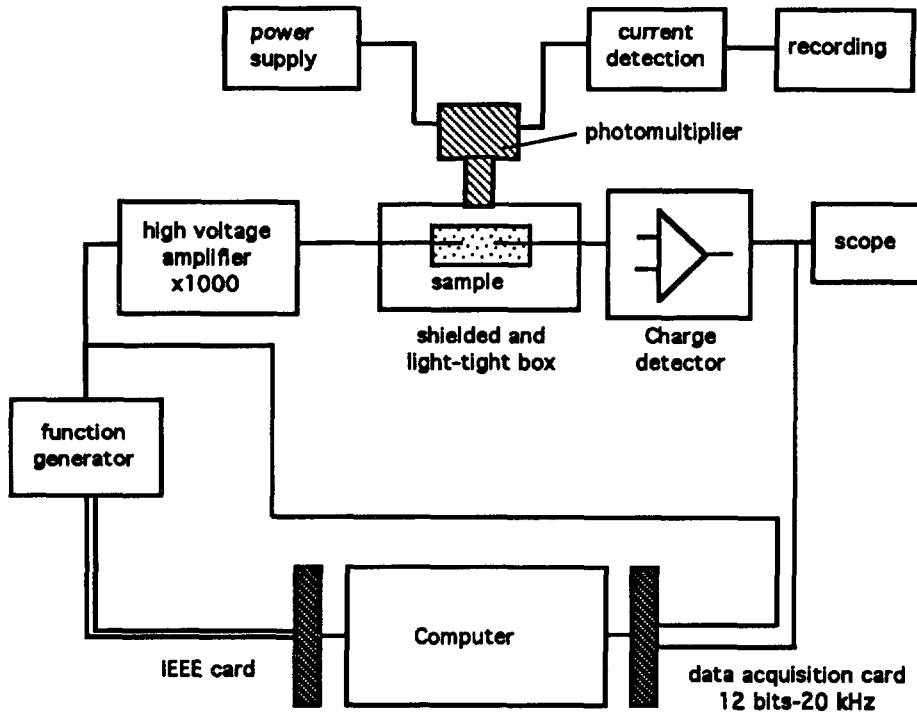


Fig. 3. — The whole set-up with optical detection.

propagation phase of treeing with light emitted from gas discharge in the first channel of a tree. Moreover, correlation can be made between electrical and optical discharge related signals.

3.3 SAMPLE PREPARATION. — Two kinds of additive-free low density polyethylene (LDPE) samples were studied, with metallic or semi-conducting electrodes. Samples with stainless steel needles were prepared by compression moulding of polyethylene pellets at 170 °C during 45 min. The needles are first cleaned, then inspected through high-power optical microscopy in order to discard any damaged ones and to measure the exact radius of curvature of the needle tip (typical value $\approx 3 \mu\text{m}$). In order to better simulate the real situation in a power cable where the insulant is not in direct contact with a metal but rather with a carbon-black doped polyethylene shield, experiments were carried out with semiconducting needles. They were realized from a cross-linked semiconducting sheets, 160 μm thick, obliquely cut to produce protrusions with a tip radius of $\approx 2 \mu\text{m}$. These were sandwiched between 150 μm thick pre-moulded polymer films and the specimen were heated at 170 °C for 35 min. The distance between the tip of the semiconducting protrusion and the blunt counter electrode was 2 mm. Both kinds of specimen are described in figure 4.

After moulding, the samples cooled down slowly to room temperature in order to minimize mechanical stress. They were also examined through optical microscopy to check for any major defect near the needle tip, such as microcavities due to poor control of the moulding process. They were then short-circuited for several days in a dry environment in order to neutralize the residual electrical charges created during moulding. All these operations were important since the properties of a given sample depend on both the quality of the moulding and its residual charge. When a microcavity is present at the needle tip, the capacitive compensation is not stable in time, probably because of the time-dependent conduction of the

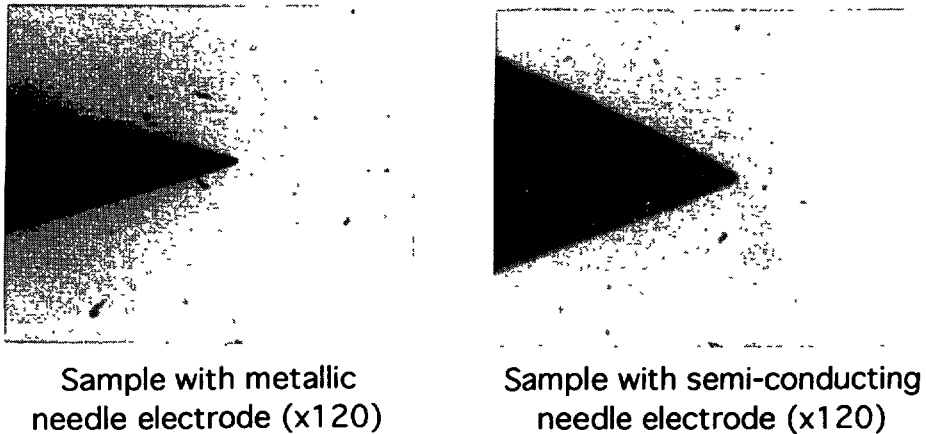


Fig. 4. — Microscopic observation of metallic and semi-conducting needle-like electrodes moulded into polyethylene.

cavity wall. Moreover, small discharges accompanied by pulsating light emission are detected at low stress levels. These two phenomena allow to detect sample defects. These methods of detection are much more reliable to check the polymer-needle interface than an observation of the specimen through an optical microscope.

4. Experimental results and discussion.

Results obtained with metallic needles are presented first. Those concerning samples with semi-conducting protrusions are described in a special section below.

4.1 SPACE CHARGE INJECTION *versus* VOLTAGE : STRONG INJECTION ONSET. — The experimental procedure was the following : the two charge components are balanced at low stress ($V = 100 V_p$), and the voltage is increased from this value to $5\,000 V_p$ by steps of $100 V_p$, the duration of each step being 5 s.

A typical experimental pattern is given in figure 5a where the peak output charge is plotted as a function of the peak voltage. The non-linear variation of the charge above V_c can be seen on the experimental plot. Below V_c , the signal is constant and constitutes the zero level of the charge detector due to electrical noise in the circuit. In accordance with the FLSC model, the square root of the charge (Fig. 5b) is linear *versus* voltage above the strong injection onset voltage V_c . The detected charge is twice as high as the theoretical value but the FLSC model gives the correct order of magnitude. For this specific sample, a critical field $E_c \approx 1.8$ MV/cm is derived from the V_c value by taking into account the needle curvature radius.

Fifty-two samples with needle tip radius ranging from $2.5 \mu\text{m}$ to $4 \mu\text{m}$ were tested following the same procedure. A few samples (5) were discarded as discharges in the 0.1 pC range were detected at low stress. As previously emphasized, this behaviour is due to defects occurring during the moulding procedure. All the forty seven remaining samples exhibit a non-linear charge-voltage characteristic. The critical fields obtained are shown on the histogram in figure 6. They scatter over a wide field range with an average value of 0.7 MV/cm. It was not possible to relate the observed scattering to a characteristic of each sample : this may be due to uncontrolled local conditions at the needle tip as it will be discussed later. The discrepancy between theoretical and measured charge is always observed.

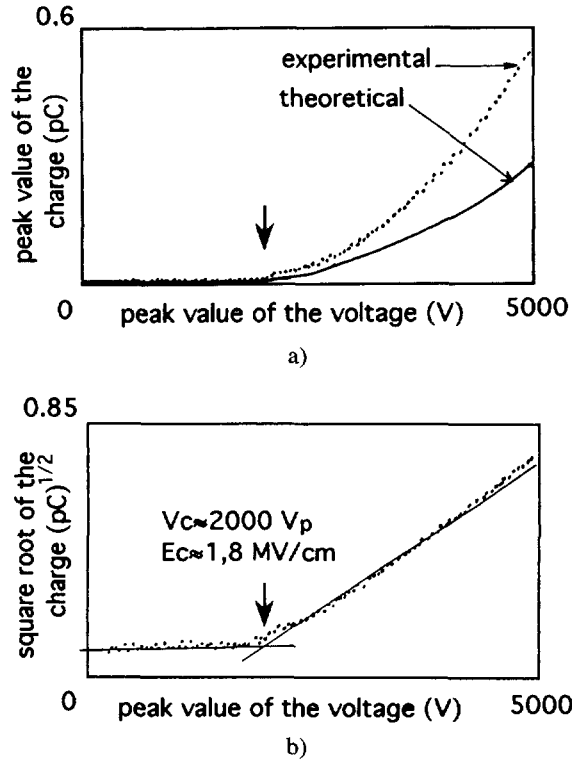


Fig. 5. — Charge injection *versus* voltage : strong injection onset. a) Charge *versus* voltage. b) Square root of the charge *versus* voltage. The quantitative agreement between the experimental and theoretical values of the charge is rather poor but the charge-voltage relationship has been established for impulse voltage. It can only constitute an estimate when applied to a.c. voltage conditions.

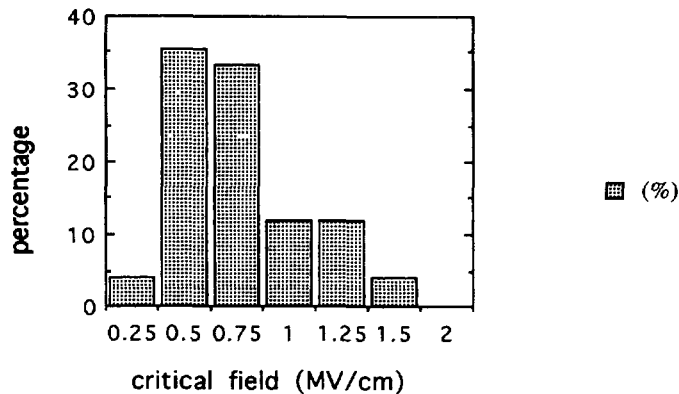


Fig. 6. — Statistical scattering of the critical fields measured on 47 samples.

4.2 CHARGE INJECTION WAVEFORM *versus* TIME IN THE DISCHARGE-FREE REGIME. — The experimental variation of charge *versus* time under a constant stress is shown in figure 7. Below the critical voltage V_c , the signal is the noise level (Fig. 7a). Above V_c , it represents the

charge waveform. When the voltage is stabilized at low overvoltage $V/V_c \approx 2$, the charge waveform presents the distinctive shape with flat maxima (Fig. 7b). A charge of about 0.1 pC is injected during each half wave. Charge injection and extraction occur during each cycle of the power frequency, and the injection current (dQ/dt) drops to zero due to field lowering at the electrode tip in relation to the amount of charge injected into the dielectric and to the lessening of the applied voltage. After several minutes under constant stress amplitude, the charge injection signal tends to be purely sinusoidal, with an increasing amplitude (Fig. 7c). This behaviour was previously reported [7, 10] and might be due to the persistence of a fraction of the injected charge deeply trapped in polyethylene. The situation at the needle tip might be

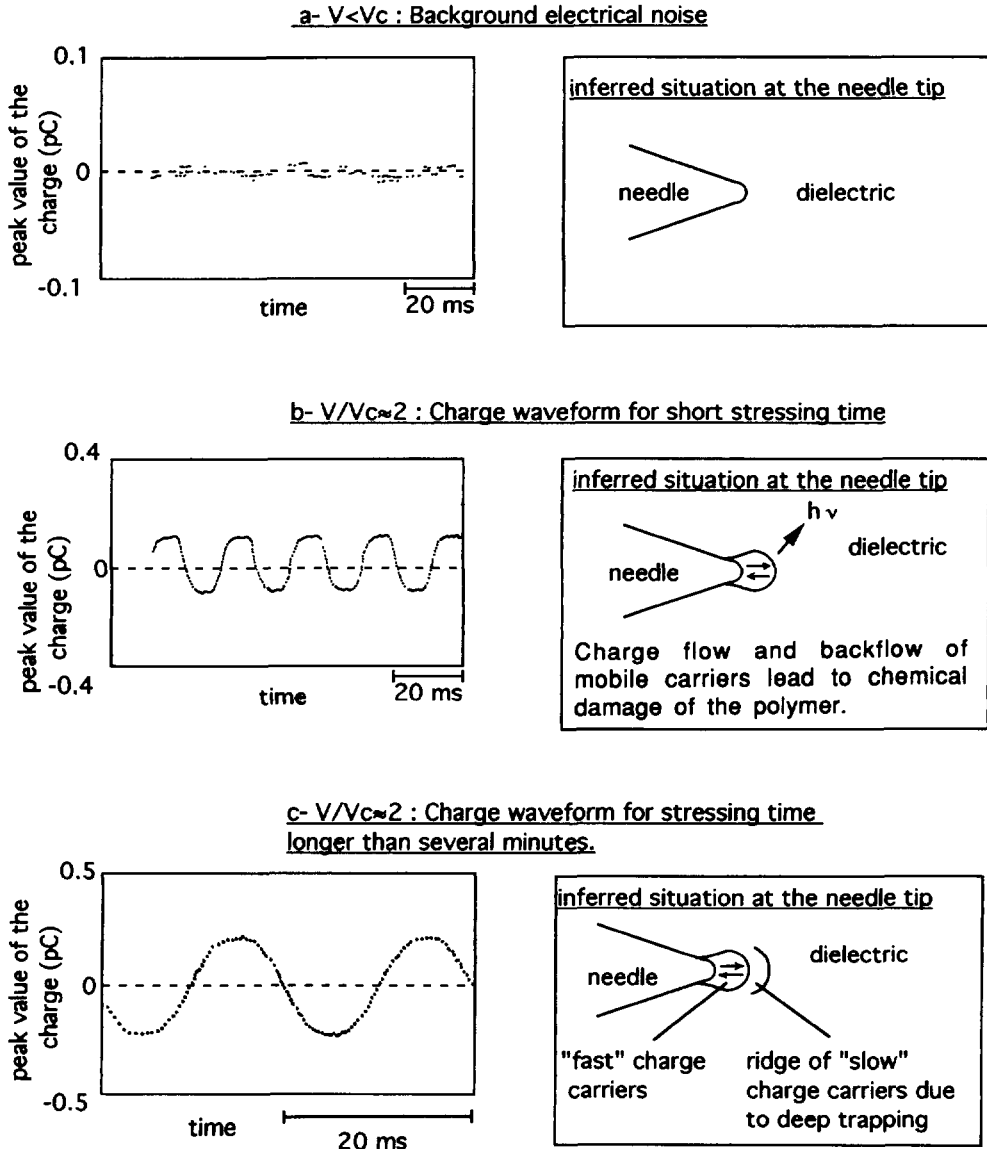


Fig. 7. — Charge waveform *versus* time under constant a.c. stressing. a) Undercritical conditions. b) Small overvoltage V/V_c , short stressing time. c) Small overvoltage V/V_c , a few minutes under stress.

depicted as follows : a flow and backflow of carriers take place around the needle and give rise to chemical degradation due to energy transfer process [11]. Light is emitted from this volume by electroluminescence (see Fig. 7b). A pure symmetrical flow and backflow of charge would give a nil residual space charge after stressing. This is indeed forecast by computer models [12] ignoring deep trapping. The effect of deep trapping would be to create a ridge of charge at the end of the « fast » carrier region (see Fig. 7c) which gradually dissipates under low mobility. This amount of charge is likely to increase with the time under stress which might explain the observed change in the charge waveform. Moreover, deep trapping is a necessary condition for electroluminescence to be emitted [4].

The evolution of the charge waveform *versus* time described above is similar to that one observed under an increasing voltage. The same interpretation is still valid.

4.3 MICRO-PARTIAL DISCHARGES IN THE TRANSITION REGIME TO ELECTRICAL TREEING. — When the sample is aged for a sufficiently long time, which obviously depends on the ratio V/V_c , high frequency phenomena begin to appear in the recordings. These discharge-like pulses are initially in the 0.05 pC range, and appear as small jumps in the charge injection signal (see Fig. 8). These very fast transients associated with these high-frequency phenomena are integrated by the charge detector and are recorded as jumps in the charge signal because of the low sampling frequency of the data acquisition card. Concomitantly, pulsating light emission is detected, which confirms the origin of the electrical signal.

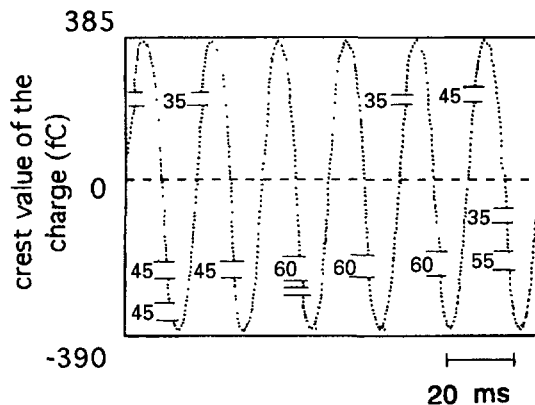


Fig. 8. — Small discharges in the 0.05 pC range during transition to electrical treeing (time to tree inception : 56 min under 5.6 kV_{rms}, 50 Hz).

The occurrence of 0.05 pC level discharges was correlated with a micrometric tree channel at the needle tip. This was discovered by cutting the sample into thin slices and inspecting the region near the needle tip through a microscope. In figure 9 electrical trees are shown at different stages of growth together with the amplitude and phase angle of small associated discharges. Our results are in accordance with the observations made by Hozumi *et al.* [13] who report discharges of 0.05 pC level in 2 μ m long tree. Further tree growth gives rise to discharges of increasing amplitudes. The time evolution of discharge magnitudes depends on both interelectrode spacing and voltage level. These partial discharge characteristics were reported in previous papers [14, 15].

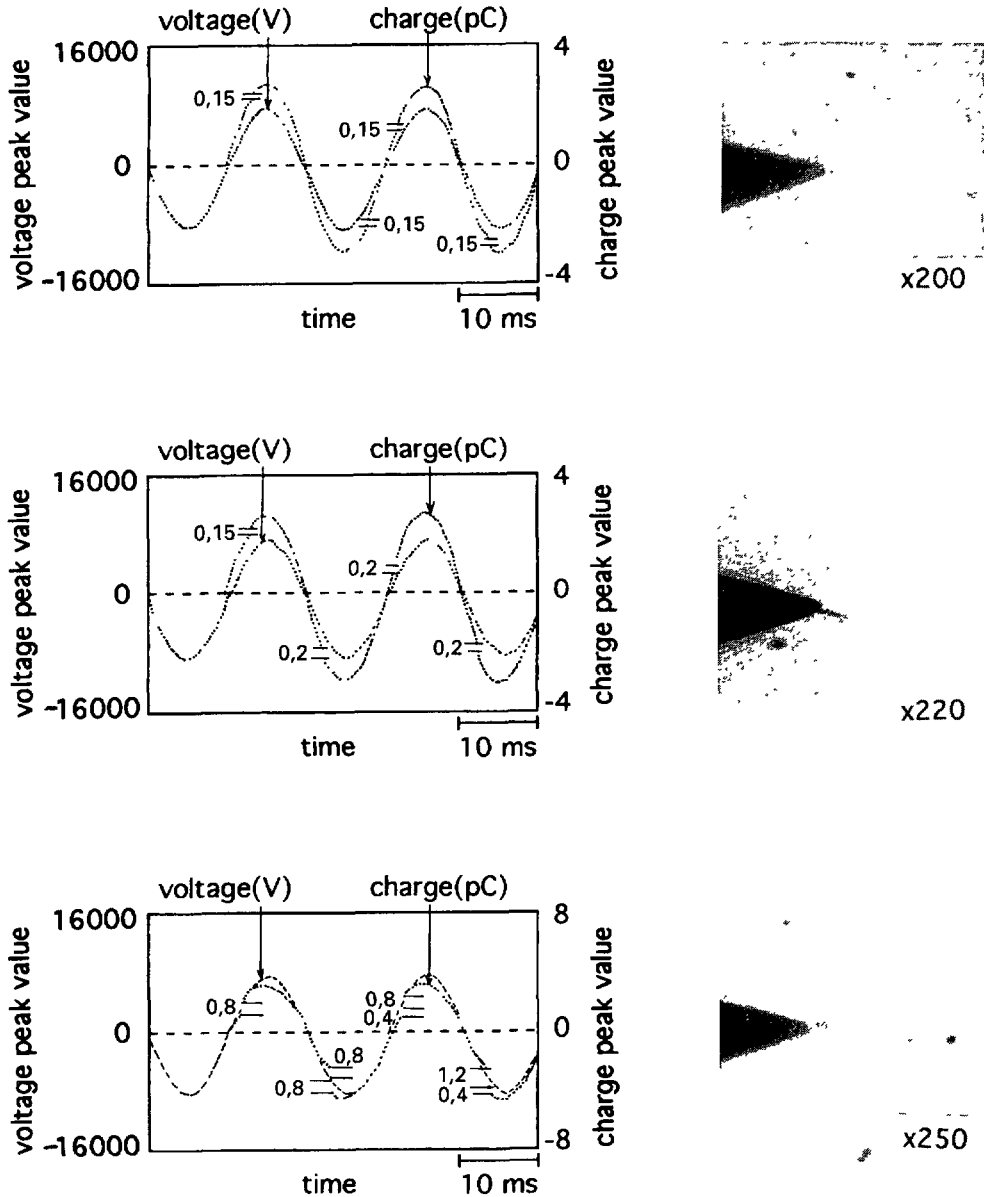


Fig. 9. — Early tree propagation phase and associated microdischarges. Charge recording begins 10 ms after time 0.

4.4 STATISTICS OF TREE INCEPTION TIME AND BREAKDOWN PATTERN. — Tree inception times under a constant stress of $7 \text{ kV}_{\text{rms}}$ were determined for each of the forty seven samples. They were derived from the time evolution of light emitted by the samples as shown in figure 10 : a very weak emission level with no discharge during the incubation period (electroluminescence [3-5]) followed by a strong unstable emission due to partial discharges in the tree up to breakdown. The incubation time is properly derived from such a plot. We have looked for correlations between individual time to tree inception and critical voltage for charge transfer

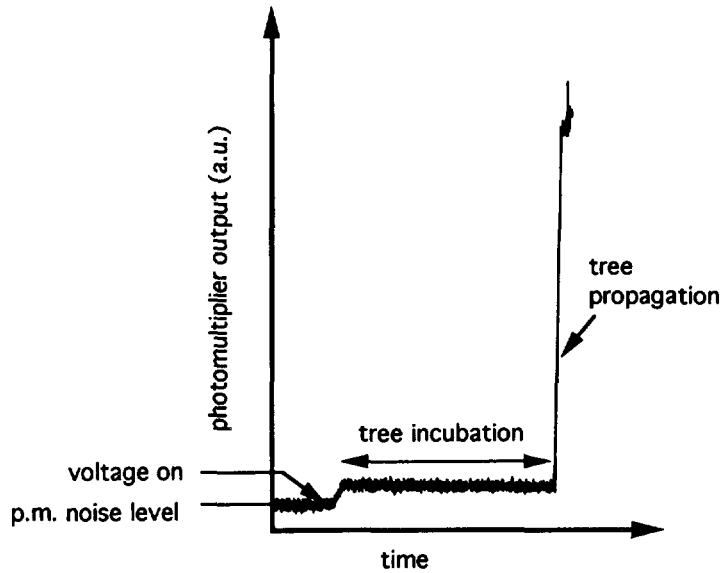


Fig. 10. — Emission of light from the sample during tree initiation and propagation phase.

for every sample of the population. The correlation degree was found to be very low (see Fig. 11). This implies that the critical field for charge transfer is not the controlling parameter in incubation process, or alternatively, that the field values derived from the critical voltages are not correct.

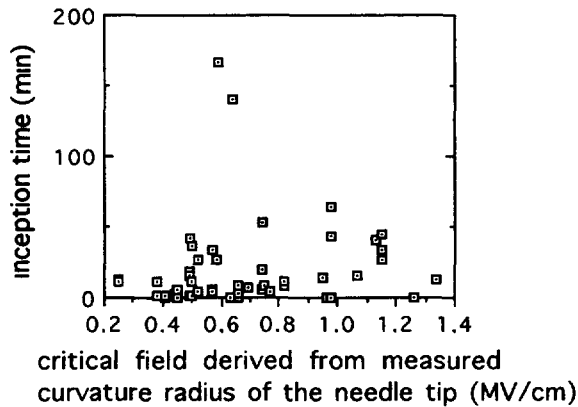
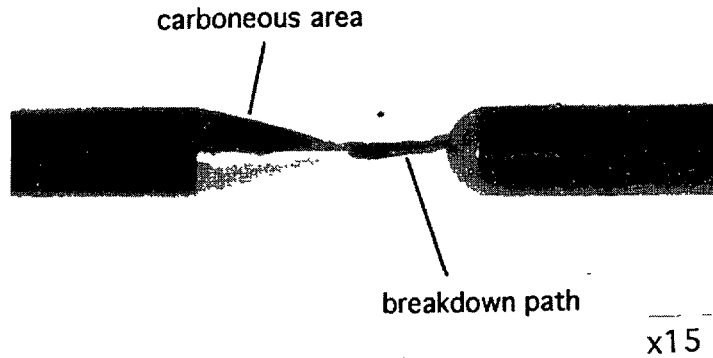
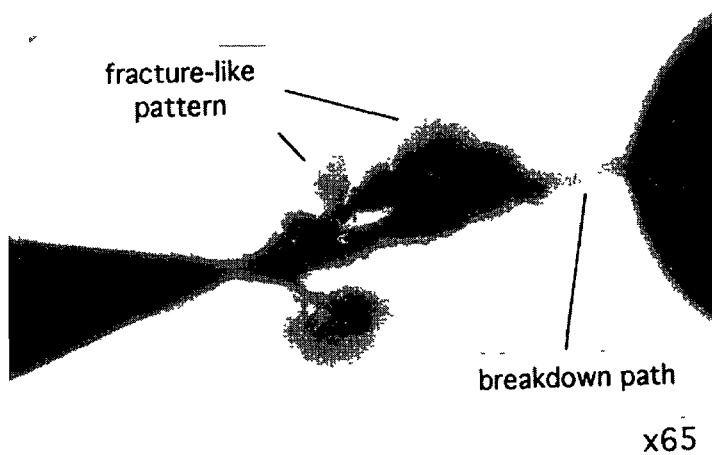


Fig. 11. — Correlation between time to tree inception (constant voltage) and critical field for charge transfer.

The breakdown patterns were also studied: they can be classified into two different categories as shown in figure 12. In the first type, the breakdown path appears as cylindrical without any specific pattern around it. A carbonaceous area is visible on the cone of the needle. In the second type, fracture-like structures spread from the cylindrical part of the breakdown



Breakdown pattern in case of bad
metal-insulator interface



Breakdown pattern when
the metal-insulator contact is tight

Fig. 12. — Classification of breakdown pattern into two different classes.

path, without any carbonization of the metallic needle surface. This demonstrates that in part of the sample (approx. 10%), the interface between polymer and metal is not so tight. Breakdown is accompanied with a strong increase in gas pressure due to the thermal shock wave. When the contact at the metal-polymer interface is tight, the gas arising from solid decomposition cracks the polymer and does not relax at this interface. On the contrary, the easy way for the gas to relax in case of a bad interface is along the needle. Therefore the

population of samples is not as homogeneous as it could be thought considering the caution taken during the samples preparation.

The data were analyzed according to a Weibull statistical model [16] with a non-zero location parameter, or threshold. A statistical description including a threshold time was shown to be more suitable to fit the data. The following Weibull parameter values were obtained with a maximum likelihood estimate :

- nominal incubation time : 1 090.8 s ;
- threshold time for incubation : 23.4 s ;
- time dispersion parameter : 0.8.

The threshold character is not well pronounced in view of the low value derived from the computation procedure. This can reasonably be attributed to the inhomogeneous character of the samples previously pointed out. In an attempt to obtain less dispersion, we subsequently prepared a limited number of specimen following basically the same procedure but by checking each preparation step with special care. Moreover, a lower electrical stress was used to increase the times to tree inception. Consequently, the transient voltage has less influence on the incubation process. A Weibull plot of the incubation times determined for an electrical stress of 5.6 kV_{rms} is given in figure 13. The appearing of a threshold time t_0 in an important

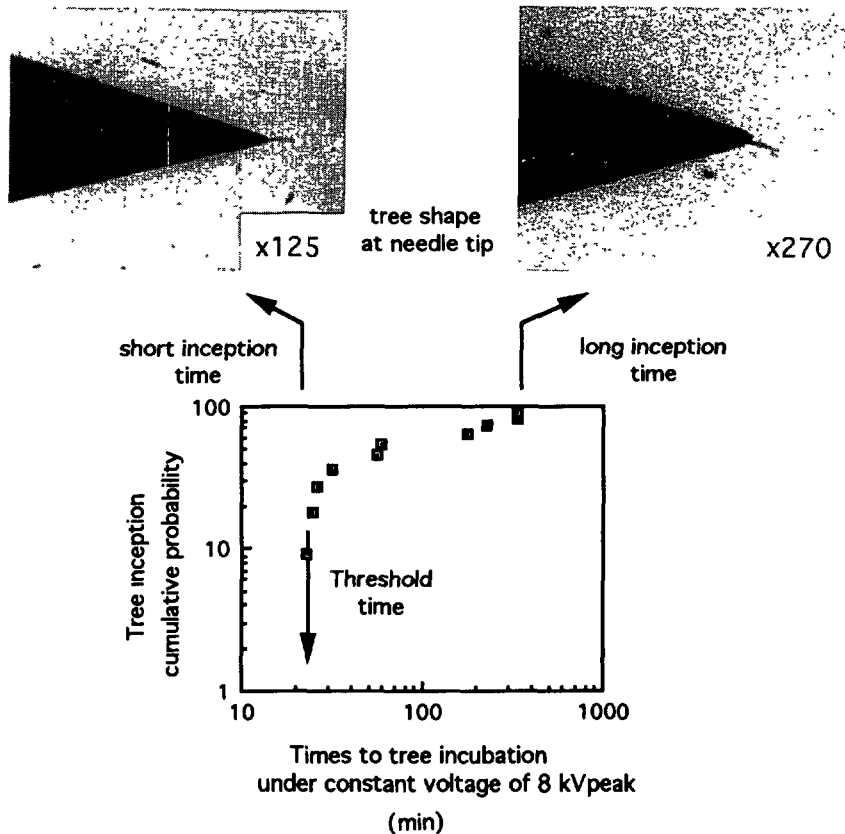
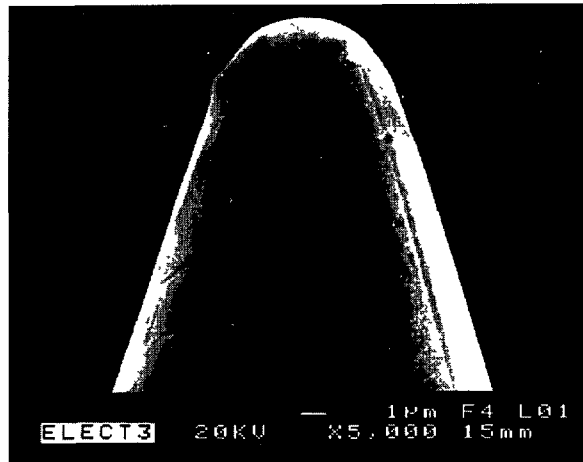


Fig. 13. — Weibull plot of times to tree inception and correlation with early tree development.

feature of the results. The best Weibull parameters obtained were as follows :

- nominal incubation time : 123 min ;
- threshold time for incubation : 23 min ;
- time dispersion parameter : 0.94.

The voltage was turned off just after tree initiation in order to visualize the tree at the needle tip in every tested sample. It turns out that in the samples with the shortest incubation times, the early tree develops at the very end of the needle whereas in samples with longer incubation times, the tree starts from the sides of the needle electrode (see Fig. 13). Uncontrolled local parameters at the needle tip seem to dominate the critical conditions allowing the tree to develop. This is further substantiated by observing a needle through scanning electron microscopy. As shown in figure 14, the surface of the metal presents irregularities which likely induced local field intensification factors over the surface. These observations are very important : they suggest that the position of injecting/extracting sites on the needle surface is an arbitrary consequence of its manufacture. The needle tip must not be considered as an homogeneous injecting surface. Moreover, it has been known for a long time that the active sites for charge transfer on a metal are small surfaces ($\approx 2\ 500\ \text{nm}^2$) [17]. Only a few of them will be active on a needle. This fact can account for discrepancies between experimental data and the simple FLSC model which assumes an homogeneous space charge cloud around the needle tip. In addition, the critical fields calculated from the nominal needle tip radius are not correct.



**Tip of a metallic needle observed with
a scanning electron microscope
(x5000)-Nominal tip radius : $3\ \mu\text{m}$**

Fig. 14. — A typical scanning electron micrograph of the surface of a metallic needle tip.

In a recent paper, Dissado and Hill [18] discussed the statistics on electrical tree inception. They propose a model which takes into account the discreteness of charge transfer site at the needle surface. The features of this model are the following : (i) charge transfer only occurs from a very small center on the surface of a needle electrode ; (ii) injection/extraction currents

above a material-dependent threshold cause damage ; (iii) a channel is formed when damage accumulates to a material-dependent critical level. Steps (ii) and (iii) are quite comparable with the process previously discussed in this paper, as the material-dependent threshold is the critical field for charge injection. Since the charge-transfer centers are distributed at random at the needle surface, the local field experienced by the active site, due to the geometrical factor of a needle-like projection, will vary according to its position. Consequently and for otherwise identical samples, the times to tree inception are statistically scattered. The appearing of a threshold time corresponding to the case where the center is located at the position of maximum field (i.e. the needle tip) is one of the main features of the results. It follows that only the threshold value can be related to the maximum field enhancement of the point.

4.5 EXPERIMENTAL RESULTS OBTAINED WITH SEMI-CONDUCTING NEEDLE ELECTRODE. — As in the case of a metallic electrode, we have studied both the non-linearity of the charge *versus* voltage and the statistics of times to tree inception. Several samples were prepared, and a selection was taken from this population on the basis of the apparent curvature radius at the tip. The selected samples have a $2\ \mu\text{m}$ curvature radius. The charge-voltage characteristics are non-linear and a critical voltage can be defined. A typical example of such a characteristic is given in figure 15. Scattering from sample to sample leads to a distribution of critical voltages but the average value of this parameter is higher ($2\ 200\ V_p$) than in the samples with metallic needles ($900\ V_p$): the charge-transfer process appears less efficient in the case of a semi-conducting electrode. This was further substantiated by studying statistics on times to tree inception. A $9\ \text{kV}_{\text{rms}}$ voltage was chosen as a stress for these tests since incubation times are far too long under a $5.6\ \text{kV}_{\text{rms}}$. A Weibull plot of the data is presented in figure 16. It reveals features similar to the ones with metallic needle, namely a strong decreasing inception probability for a short time range denoting a threshold time. This is in accordance with the finding by Dissado and Hill who argue that the form of the inception statistics obtained remains qualitatively the same for any sharp point.

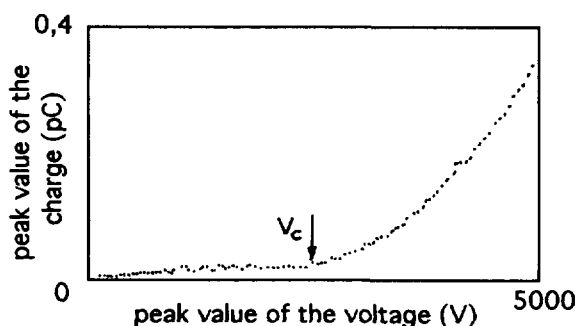


Fig. 15. — Non-linear charge-voltage characteristic of a sample with a semi-conducting needle electrode.

5. Conclusion.

We investigated electrical ageing of polyethylene used as insulation of power cables. One of the situation of interest in the context of long term performance of synthetic high voltage insulation used under a.c. stress concerns discharge-free conditions under divergent field.

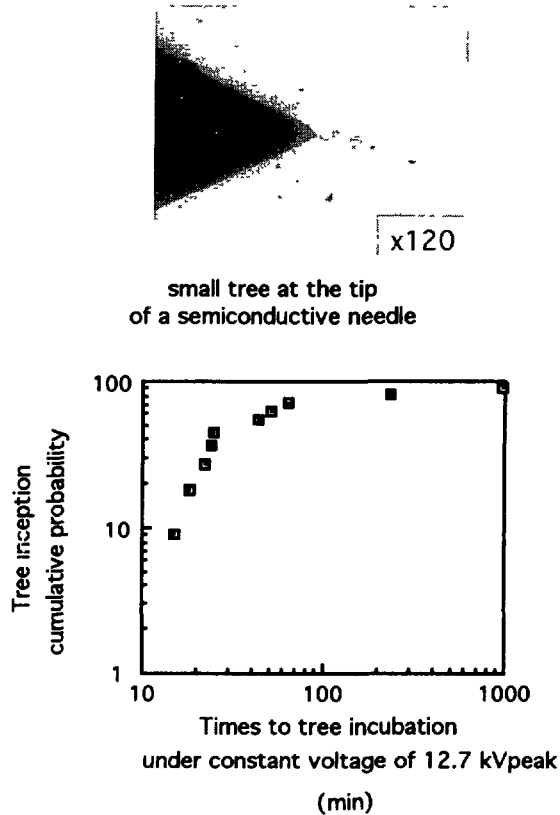


Fig. 16. — Weibull plot of times to tree inception in the case of a semi-conducting needle electrode.

Breakdown occurs by treeing which develops after a sufficient ageing period if certain critical conditions are fulfilled. Our investigation starts from the following :

- (i) charge generation above a material-dependent threshold causes damage. These charges can be supplied from the polymer bulk (i.e. field-induced carrier release) or injected into it. Electroluminescent emission is a strong experimental evidence for this phenomenon ;
- (ii) a tree is generated when the cumulative damage reaches a critical level.

By considering the average working gradient of polyethylene insulated power cables (10 to 15 kV/mm), it appears clear that electrical ageing under dry environment needs a field intensification factor to occur. This situation is simulated by using needle electrodes. Semi-conducting needles prepared from the shield of a power cable were also used in our investigation with the aim to better approach the structure of cables.

In order to detect the onset for massive charge transfer from the needle electrode into the polymer, and to investigate the transition to electrical treeing, we have built a detector with a sensitivity down to 0.01 pC. The measurement relies on the compensation of the capacitive component of the current under low voltage, and on the study of the response of the sample *versus* voltage.

The discharge-free regime (inception phase of treeing), was studied under ramped and constant stresses. Charge injection leads to a strong non-linear contribution of the total charge of the sample. This was observed on samples with metallic and semi-conducting needle

electrodes. A critical voltage for charge build-up can be derived : it separates the low from the strong injection regimes. The theoretical framework is the Field-Limiting Space Charge model which allows computation of the injected charge without knowing any transport parameters of the polymer.

The transition to electrical treeing was detected through the appearing of small discharges in the 0.01 pC range.

The quantitative agreement between the theoretical and experimental injected charge is rather poor. Moreover, no definite correlation was found between individual critical voltage and inception time. With the help of inception time statistics and microscopic observations of treed samples, the following was concluded :

- the needle tip cannot be considered as a homogeneous injecting surface. Charge transfer is controlled by small area at the needle surface ;

- statistics on times to tree inception can be explained by considering the position of defects at the needle surface relative to the tip. Only the threshold value, i.e. the minimum time to tree inception, can be related to material quality.

The real situation in needle test experiments involving polymers cannot be precisely described using a Field-Limiting Space Charge model. Three features of the model are too simplistic :

- the tip is not a homogeneous injecting surface due to defects at a microscopic scale. The fields derived from the critical voltage are not exact ;

- transition from low to high mobility is not so abrupt. The onset for non-linear behaviour is smeared out ;

- semi-cristalline polymer like polyethylene is not a homogeneous material. Since typical dimension of spherulites is similar to the space charge volume, a microscopic description of material electrical properties is needed to fully interpret the observed behaviour.

Acknowledgements.

Thanks must be expressed to Câbles-Pirelli-France and Electricité de France for their financial support.

We also wish to thank Jérôme Lefèbvre for stimulating discussions.

References

- [1] Laurent C., Mayoux C. and Sergent A., Electrical breakdown due to discharges in different types of insulations, *IEEE Trans. Elect. Insul.* **15** (1981) 33.
- [2] Zeller H. R. and Schneider W. R., Electrofracture mechanics of dielectric aging, *J. Appl. Phys.* **56** (1984) 455.
- [3] Lebey T. and Laurent C., Charge injection and electroluminescence as a prelude to dielectric breakdown, *J. Appl. Phys.* **68** (1990) 282.
- [4] Bamji S. S., Bulinski A. T. and Densley R. J., Threshold voltage of luminescence and electrical tree inception in low density polyethylene, *J. Appl. Phys.* **63** (1988) 5841.
- [5] Laurent C., Mayoux C. and Noel S., Dielectric breakdown of polyethylene in divergent field : role of dissolved gases and electroluminescence, *J. Appl. Phys.* **54** (1983) 1532.
- [6] Hibma T. and Zeller H. R., Direct measurement of space charge injection from a needle electrode into dielectrics, *J. Appl. Phys.* **59** (1986) 1614.
- [7] Lebey T. and Laurent C., Mesure du courant d'injection de charge dans les diélectriques solides sous tension alternative, *Rev. Phys. Appl.* **25** (1990) 423.
- [8] Lampert M. A. and Mark P., Current injection in solids (Academic Press, New York and London, 1970).

- [9] Griac J., Adamec V. and Calderwood J. H., On the comparability of single and double needle tests for treeing resistance, *IEEE Trans. Elect. Insul.* **17** (1982) 356.
- [10] Baumann Th., Fruth B., Stucky F. and Zeller H. R., Field-enhancing defects in polymeric insulators causing dielectric ageing, *IEEE Trans. Elect. Insul.* **24** (1989) 1071.
- [11] Cartier E. and Pfluger P., Detection of hot electron-induced radiation damage in organic dielectrics by exoelectron emission from thin films, *IEEE Trans. Elect. Insul.* **22** (1987) 123.
- [12] Hare R. and Budd C., Modelling space charge and field in solid dielectrics, IEE Conference on Dielectric Materials, Measurements and Applications (1992) p. 81.
- [13] Hozumi N., Okamoto T. and Fukagawa H., Simultaneous measurement of microscopic image and discharge pulses at the moment of electrical tree initiation, *Jpn J. Appl Phys.* **27** (1988) 572.
- [14] Laurent C. and Mayoux C., Analysis of the propagation of electrical treeing using optical and electrical methods, *IEEE Trans. Elect. Insul.* **15** (1980) 33.
- [15] Densley R. J., An investigation into the growth of electrical trees in XLPE cable insulation, *IEEE Trans. Elect. Insul.* **14** (1979) 148.
- [16] Chauvet C. and Laurent C., Weibull statistics in short-term dielectric breakdown of thin polyethylene films, *IEEE Trans. Elect. Insul.* **28** (1993) 18.
- [17] Forster E. O., The metal/liquid interface : the charge injection process, *IEEE Trans. Elect. Insul.* **19** (1984) 524.
- [18] Dissado L. A. and Hill R. M., The statistics of electrical tree inception, *IEEE Trans. Elect. Insul.* **25** (1990) 660.